

## Article

# Spatial Distribution and Factors Influencing the Various Forms of Iron in Alluvial–Lacustrine Clayey Aquitard

Juan Chen <sup>1</sup>, Rui Liu <sup>2,\*</sup>, Yantao Jian <sup>1</sup> and Teng Ma <sup>3,4</sup>

<sup>1</sup> Hebei Key Laboratory of Environment Monitoring and Protection of Geological Resources, Hebei Geological Environment Monitoring Institute, Shijiazhuang 050021, China; chenjuan\_work@126.com (J.C.); jianyantao@126.com (Y.J.)

<sup>2</sup> China Institute of Geo-Environment Monitoring, Beijing 100081, China

<sup>3</sup> School of Environmental Studies, China University of Geosciences, Wuhan 430078, China; mateng@cug.edu.cn

<sup>4</sup> State Environmental Protection Key Laboratory of Source Apportionment and Control of Aquatic Pollution, China University of Geosciences, Wuhan 430078, China

\* Correspondence: hjiurui0225@163.com

**Abstract:** The compression release of pore water in clayey aquitards has a significant impact on groundwater quality. Iron is an active variable element that mediates biochemical reactions in groundwater systems, but its transformation mechanisms in clayey aquitards remain unclear. The sediment and pore water samples from the shallow clayey aquitard (thickness = ~20 m) in the Chen Lake area of China were collected in three boreholes. The spatial distribution and influencing factors of Fe occurrence in the aquitard were revealed using hierarchical extraction, statistical analysis, and simulation calculations. The results indicate that the background value of alluvial–lacustrine sediments primarily affects the Fe concentration of clayey sediments. The dissimilatory reduction in free Fe oxide was the main source of Fe ions in pore water, resulting in a major percentage of Fe<sup>2+</sup> in the total Fe concentration (0.07–5.91 mg/L). The abundant organic matter in organic-rich clay promoted a dissimilatory reduction in Fe (III) oxides, while the Fe concentrations of sediment and pore water were lower in the sand-rich stratum because of its weak adsorption capacity. The impact of human reclamation activities on the aquitard was mainly concentrated in the shallow layer (> –3 m), resulting in water drainage and O<sub>2</sub> and CO<sub>2</sub> input, which induced the crystallization of poorly crystalline Fe oxides. The input of reactive organic matter from reclaimed crops promoted the dissimilatory reduction in Fe oxides and the enrichment of Fe in deep pore water. The copious Fe<sup>2+</sup> in deep stratum pore water tended to interact with CO<sub>3</sub><sup>2-</sup> and S<sup>2-</sup> to form coprecipitation with Fe (II). The concentrations of As, Cr, Sr, Zn, and Mn in pore water followed a similar variation trend to the Fe ion concentration, and their release could be attributed to the reduction dissolution of sediment Fe (III) oxides.

**Keywords:** clayey aquitard; sediment; pore water; iron form; spatial distribution



**Citation:** Chen, J.; Liu, R.; Jian, Y.; Ma, T. Spatial Distribution and Factors Influencing the Various Forms of Iron in Alluvial–Lacustrine Clayey Aquitard. *Water* **2023**, *15*, 3934. <https://doi.org/10.3390/w15223934>

Academic Editor: Bahram Gharabaghi

Received: 14 October 2023

Revised: 6 November 2023

Accepted: 9 November 2023

Published: 11 November 2023



**Copyright:** © 2023 by the authors. Licensee MDPI, Basel, Switzerland. This article is an open access article distributed under the terms and conditions of the Creative Commons Attribution (CC BY) license (<https://creativecommons.org/licenses/by/4.0/>).

## 1. Introduction

The effect of aquitard on groundwater safety has raised widespread concern around the world [1–4]. The clayey sediment is a common aquitard in plains, formed by the evolution of loose surface sediments with a high moisture content [5]. Complex water–rock interactions occur inside the clayey sediments, and abundant chemical substances are released into adjacent aquifers with pore water via advection, diffusion, or compaction, affecting groundwater quantity and quality [6]. Many studies have discovered that a large portion of groundwater originates from clayey aquitards [7,8]. Smith et al. found that the discharge of clay pore water during clayey sediment compaction is closely related to the formation of groundwater with high arsenic concentrations in California, USA [9]. Jiao et al. discovered a considerable amount of releasable ammonium stored in the clayey aquitards of

the Pearl River Delta groundwater system [2]. Li et al. found that the compression-released clay pore water with high fluoride levels could enrich the groundwater fluoride in the North China Plain [10]. Therefore, the release of pore water during the evolution of clayey aquitards may have a potential impact on the water quality of adjacent aquifers, and the water–rock interaction is an important cause of the formation of problematic components in pore water.

Iron (Fe) is the fourth most abundant element in the crust and a key element controlling biogeochemistry and redox reactions in groundwater systems [11]. Fe is one of the terminal electron receptors of microbial reactions, facilitating the migration and transformation of other essential elements (such as carbon, nitrogen, phosphorus, etc.) [12–15]. The reductive dissolution of Fe (hydrogen) oxides is an important process for the release of Fe-bound contaminants such as heavy metals [16,17]. The intense reduction environment and high levels of organic matter (OM) regulate the reduction reaction and secondary mineral types of Fe (hydrogen) oxides in clayey aquitards [3,18,19], resulting in the release of Fe-bound elements such as arsenic [9,20]. Due to inelastic compaction and advection, anaerobic metabolites such as Fe (II), Mn (II), or dissolved organic carbon (DOC) can enter the aquifer with clay pore water, mediating the anaerobic conditions of adjacent aquifers [21]. Elevated Fe levels in groundwater can cause a variety of issues, including the unsatisfactory taste of drinking water and irrigation system blockage [22]. Therefore, identifying the occurrence characteristics and influencing factors of Fe in clayey aquitards is critical for understanding the Fe cycle in groundwater systems and the formation mechanism of inferior natural groundwater. However, due to the low-water supply capacity of aquitards in the traditional view, relevant research has remained limited.

Jiangnan Plain (JHP) is located in southeast China and was formed by the alluviation of the Yangtze and Han Rivers. The JHP is an important commodity as a grain, cotton, and oil production base in China. Groundwater is a key source of the water supply in the JHP. Warm paleoclimatic conditions following the last glacial period led to intense alluvial–lacustrine deposition, resulting in a laterally spread and extensively dispersed dark-brown clayey aquitard [23]. After a lengthy period of water–rock interactions and biochemical reactions in this area, the pore water within the thick clayey sediment could become a natural source of inferior components in aquifer groundwater. High levels of Fe up to 32.2 mg/L have been detected in the Pleistocene aquifers of the JHP [24], which is significantly higher than the World Health Organization’s (WHO’s) guideline limit (0.3 mg/L). Previous studies have linked the reduction dissolution of clayey sediment Fe (III) to the enrichment of As, Cr, and P in JHP Quaternary groundwater [25–27]. However, the migration and transformation processes of clayey sediment Fe in JHP remain unknown.

Hence, the purpose of this study is to identify the occurrence characteristics and factors that influence the various forms of Fe in alluvial–lacustrine clayey aquitard. Chen Lake wetland is located in the eastern region of the JHP. Considering the influence factors of natural and human activities, the Chen Lake wetland containing the lake and reclamation areas was selected as the study area. The borehole sediments and pore water samples from the shallow clayey aquitard were collected, and the occurrence of Fe was analyzed via hierarchical extraction, statistical analysis, and simulation calculation. The issues addressed in this paper could be generally applicable to other Quaternary alluvial–lacustrine aquifer systems around the world.

## 2. Study Area

The Chen Lake wetland (30°15′–30°27′ N, 113°46′–113°53′ E; about 269 km<sup>2</sup>) is located in the eastern part of the JHP, Eastern China (Figure 1a). The Chen Lake wetland has a sub-tropical monsoon climate with an average annual temperature of 16.5 °C and an average annual precipitation of 1250 mm. The landscape of Chen Lake wetland belongs to the flat plain type, which is a low-lying area formed by the confluence of the Yangtze and Han Rivers. The ground elevation ranges from 17.5 to 21.0 m above sea level, and the

underlying strata of Chen Lake are the most common alluvial–lacustrine facies strata in the JHP.

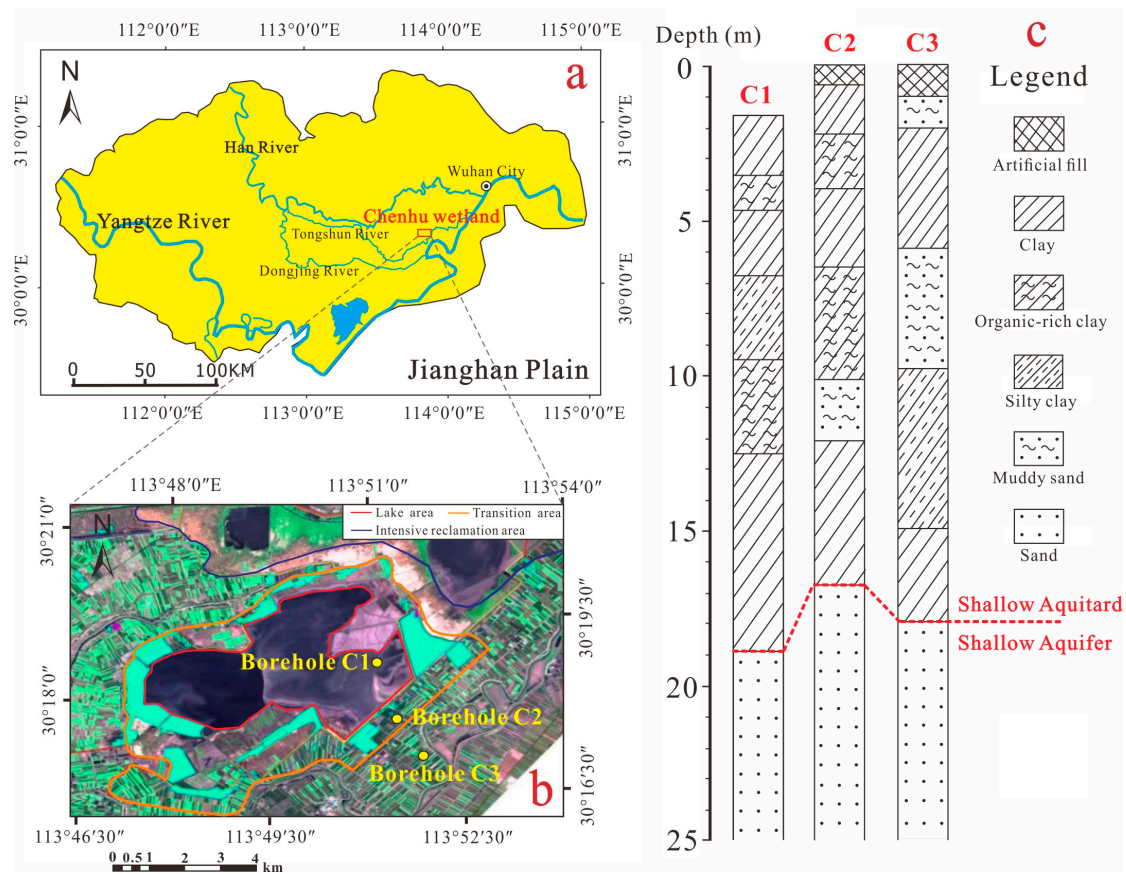


**Figure 1.** The geographic location and lithologic profiles of the study area. (a) Location of Chen Lake wetland in the eastern part of JHP. (b) Locations of boreholes C1, C2, and C3 in Chen Lake wetland. (c) Lithologic profiles of three boreholes.

The surface sediments in the Chen Lake area are composed of Upper Pleistocene ( $Q_p^3$ ) or Holocene ( $Q_h$ ) alluvial–lacustrine sediments and Quaternary unconsolidated sediments form a porous medium for groundwater storage and flow. The groundwater system structure of the Chen Lake wetland is divided into a shallow aquitard, a shallow aquifer, a deep aquitard, and a deep confined aquifer [23,28]. The shallow aquitard is composed of Holocene silt and clay with a thickness of 15–30 m and a hydraulic conductivity of  $10^{-10}$ – $10^{-9}$  m/s. The shallow aquifer, one of the main sources of local water supply, is composed of Late Pleistocene fine- to coarse-grain sand and gravel with a thickness of 50–80 m and a hydraulic conductivity of  $10^{-8}$ – $10^{-7}$  m/s [29]. This research focuses on the occurrence and fate of Fe in the shallow aquitard.

Reclamation involves the transformation of natural lakes and other wetlands into cultivated or other land types, which is a typical representation of how human activities transform nature. Reclamation changes the topography and hydrological cycle of lakes, which may have an impact on the Fe cycle in lake–groundwater systems. Therefore, reclamation was considered as artificial influence factor of Fe migration and transformation in clayey aquitards. The reclamation of Chen Lake was conducted by erecting barriers to hold back the lake and draining the lake water near the shore, and then the exposed land areas were reclaimed and cultivated. Chen Lake has been reclaimed by enclosing the lake district from the edge to the center for cultivation since the 1950s (Figure 1b). Chen Lake has changed from an open-type lake to an independent, closed aquaculture lake in modern times. The underlying sediments were formed under different hydrodynamic conditions.

The shallow aquitard sediments of Chen Lake wetland experienced the same deposition process and had similar soil parent material. Except for the effect of cultivated crops, there was no significant disturbance from other exogenous substances in the underlying aquitard.

### 3. Methodology

#### 3.1. Sample Collection and Water Level Monitoring

Sediment samples from the clayey aquitard at different depths were collected through three boreholes arranged in the lake area, transition area, and intensive reclamation area (Figure 1b). Borehole C1 is located within the Chen Lake area, which is affected less by human activities. Borehole C3 is located in an intensive reclamation area with a 50-year history of rice and corn cultivation. Borehole C2 is located in the midway transition area from the edge to the center of the ancient lake, with a lower degree and shorter time of reclamation than borehole C3. Three monitoring holes (depths: −5 m, −10 m, and −20 m) were set around each borehole.

From each borehole in the shallow clayey aquitard, a 15 cm sediment core was collected at depth intervals of 1.0 m. The samples were wrapped with preservative film and aluminum foil to isolate air and light and were then placed into PVC pipes to prevent extrusion. The sediment samples were transported to the laboratory and stored in the refrigerator at 4 °C. A total of 52 sediment samples were collected (borehole C1: 18, borehole C2: 16, borehole C3: 18). Pore water samples (a total of 52) were collected using a specific compaction experimental device [30]. The water levels of lake water around borehole C1 and groundwater in all monitoring holes were measured manually by an electronic water sensor every two weeks from April 2019 to January 2020 to identify the vertical hydraulic conductivity processes. The groundwater samples from monitoring holes were collected and measured to identify the input differences of surface materials in the deep environment of clayey aquitards.

#### 3.2. Measurement Methods

##### (1) Sediment samples

The total Fe content of sediment samples was measured via X-ray fluorescence spectrometry (E-max 500). Three different forms of Fe oxides were identified using chemical extractions (Table 1). In each extraction experiment, 0.5 g from each sample was weighed and put into a 50 mL centrifuge tube. A total of 30 mL of extractant was added to the centrifuge tube and shaken for 16 h, then centrifuged at room temperature for 2 h at  $5300 \times g$ . Each extraction was performed twice, and the results were kept as pseudo-replicates [31]. The concentrations of Fe ions in the extractions were measured via ICP-OES (PerkinElmer Avio 200, Waltham, MA, USA).

**Table 1.** Extractable phases of Fe oxides and conditions, adapted from [31].

Dissolution Solvent	Solvent Molarity	Solvent pH	Target Phases	Dissolution Mechanism
Dithionite-HCl	0.05 M, 0.05 M	3–4	Crystalline Fe (III) oxides, poorly crystalline Fe (III) oxides	Reduction
Ammonium oxalate	0.2 M	3	Poorly crystalline Fe (III) oxides	Chelation
Sodium pyrophosphate	0.1 M	~10	Colloidal or OM-chelated Fe	Dispersion, chelation

The free Fe (III) oxides (mainly including crystalline Fe oxides, containing parts of poor crystalline Fe oxides) were commonly estimated by dithionite-HCl (DH) extraction [32]. The free Fe oxide is represented by  $Fe_{DH}$ .

The amorphous or poorly crystalline Fe (III) oxides had large specific surface areas and high activity and were extracted using an ammonium oxalate (AO) buffer solution ( $(NH_4)_2C_2O_4$ ) [33]. The extraction process was achieved via the chelation of poorly crystalline Fe and oxalic acid. The amorphous Fe oxide is represented by  $Fe_{AO}$ .

The colloidal or OM-chelated Fe oxides were extracted via a sodium pyrophosphate solution ( $\text{Na}_4\text{P}_2\text{O}_7 \cdot 10\text{H}_2\text{O}$ , PP) [34]. Sodium pyrophosphate can disperse the Fe–OM complex and then combine with Fe. The OM-chelated Fe oxide is represented by  $\text{Fe}_{\text{PP}}$ .

Residual sediment Fe minerals are mostly found in layered silicates, which have low activity and rarely enter groundwater through water–rock interactions. Therefore, this part of Fe is not discussed in this paper.

The stoving method was used to determine the moisture content of sediment samples (the mass ratio of liquid to solid). The total organic carbon (TOC) contents of sediment samples were measured using a TOC analyzer (Elementar Vario TOC, Frankfurt, Germany).

## (2) Pore water samples

The pH, redox potential (Eh), electroconductivity (EC), and dissolved oxygen (DO) of pore water released from the sediment were tested using an Orion water quality analyzer with an ion-selective electrode (Thermo-Fisher Scientific Orion Versa Star, Waltham, MA, USA). The alkalinity was determined via hydrochloric acid titration. The cation and anion standard solutions were obtained from O2Si Company Limited (North Charleston, SC, USA). The pore water anions were measured via ion chromatography (Thermo Fisher Scientific ICS 1100, Waltham, MA, USA) and cations via ICP-OES (PerkinElmer Avio 200, Waltham, MA, USA) after filtration using  $0.45 \mu\text{m}$  filter membranes. The dissolved organic carbon was measured using a TOC analyzer (Elementar Vario TOC, Frankfurt, Germany) (limit of quantification:  $0.01 \text{ mg/L}$ ). Pore water samples were first filtrated using  $0.22 \mu\text{m}$  filter membranes and treated with sufficient phosphoric acid to remove inorganic carbon before the DOC measurement. Trace elements (heavy metals) were measured via ICP-MS (PerkinElmer Nexion 350D, Waltham, MA, USA). The concentration of  $\text{Fe}^{2+}$  and  $\text{S}^{2-}$  in pore water was determined using a HACH 2801 ultraviolet spectrophotometry (Loveland, CO, USA). Dissolved inorganic carbon (DIC) concentrations were calculated according to alkalinity. Three groups of parallel samples were set for each test.

Stable C isotopic compositions ( $\delta^{13}\text{C}$ ) of sediment TOC and pore water DOC were analyzed via Vario cube TOC-isoprime 100 (Elementar, Frankfurt, Germany) with a precision of  $\pm 0.2\text{‰}$  at the Third Institute of Oceanography, Ministry of Natural Resources.

The fluorescence characteristic of dissolved organic matter (DOM) in pore water was determined using a Hitachi F–4500 spectrometer (Tokyo, Japan). Emission (EM) spectra were scanned from 200 to 550 nm at 5-nm intervals with 2-nm increments of the excitation (EX) from 300 to 600 nm.

## 4. Results

### 4.1. Variation in Fe Oxide Contents with Depth

According to the test results, the average values of the basic physicochemical indicators of sediment and pore water at different depths are listed in Table 2. The variation in concentrations of Fe oxides in sediment samples and total Fe and  $\text{Fe}^{2+}$  in pore water samples with depth is shown in Figures 2–4.

The research area was in the alluvial–lacustrine facies strata with complex lithological changes. Different types of sediment have distinct chemical substance background values, such as muddy sediments with higher TOC concentrations than adjacent layers (Table 2). Due to the compression–release of pore water, the moisture contents in all three boreholes decreased with depth. The sediment Fe oxide concentration accounted for 29.23–46.02% of the total Fe and decreased with depth, indicating that the predominant migration and transformation occurred in Fe oxides, whereas the structural Fe in silicates was relatively stable.

The  $\text{Fe}_{\text{DH}}$ ,  $\text{Fe}_{\text{AO}}$ , and  $\text{Fe}_{\text{PP}}$  contents of borehole C1 sediments were 9.42–22.51 (~average value = 16.76), 8.36–37.86 (~average value = 17.20), and 0.22–3.72 (~average value = 0.70) mg/g, respectively. Overall, the  $\text{Fe}_{\text{DH}}$  content decreased with depth, which was higher than the  $\text{Fe}_{\text{AO}}$  content in shallow strata but was overtaken by the  $\text{Fe}_{\text{AO}}$  content below –6 m. The  $\text{Fe}_{\text{PP}}$  content was relatively low, and it increased in the organic-rich clay layer due to the high TOC content (Figure 2).

**Table 2.** Lithology and average levels of moisture content, total Fe, and TOC in sediment samples and average levels of pH and Eh of pore water samples at different depths.

Borehole C1 Depth (m)	Lithology	Moisture Content (%)	Total Fe (mg/g)	TOC (mg/g)	pH	Eh (mV)
1.5–3.5	Clay	42.40	69.04	10.09	7.854	216.0
3.5–4.7	Organic-rich clay	39.71	80.74	15.24	7.636	60.5
4.7–6.8	Clay	39.15	96.37	4.39	7.746	−56.8
6.8–9.5	Silty clay	30.40	77.74	4.20	7.692	−62.7
9.5–12.5	Organic-rich clay	34.80	83.23	6.93	7.706	−70.3
12.5–18.8	Clay	33.48	113.43	4.99	7.517	−82.2
Borehole C2 Depth (m)	Lithologic	Moisture content (%)	Total Fe (mg/g)	TOC (mg/g)	pH	Eh (mV)
0–0.5	Artificial fill	30.30	64.12	7.93	6.732	297.0
0.5–2.2	Clay	41.30	78.86	9.24	7.106	317.0
2.2–5.0	Organic-rich clay	44.40	108.49	14.95	7.231	101.0
5.0–6.6	Clay	40.03	92.47	7.97	7.430	−64.3
6.6–10.1	Organic-rich clay	36.57	110.39	8.42	7.297	−67.3
10.1–12.2	Muddy sand	37.60	77.71	11.43	7.453	−84.5
12.2–16.6	Clay	28.38	135.97	5.34	7.536	−79.0
Borehole C3 Depth (m)	Lithologic	Moisture content (%)	Total Fe (mg/g)	TOC (mg/g)	pH	Eh (mV)
0–1.0	Artificial fill	31.50	79.96	15.84	6.670	282.0
1.0–2.0	Muddy sand	40.30	82.47	11.09	6.891	244.0
2.0–6.0	Clay	37.67	73.97	10.65	7.025	−11.7
6.0–9.7	Muddy sand	35.93	92.19	5.59	7.326	−66.3
9.7–14.9	Silty clay	31.82	98.34	5.25	7.614	−53.2
14.9–18.3	Clay	27.60	88.43	3.47	7.299	−89.0

The  $Fe_{DH}$ ,  $Fe_{AO}$ , and  $Fe_{PP}$  contents of the borehole C2 sediments were 5.75–30.66 (~average value = 19.63), 3.72–41.11 (~average value = 20.09), and 0.36–1.89 (~average value = 0.87) mg/g, respectively. The overall contents of Fe oxides in various forms of borehole C2 were higher than those of borehole C1. The  $Fe_{DH}$  content decreased in fluctuation with the depth, and the  $Fe_{AO}$  content exceeded the  $Fe_{DH}$  content at a depth of about −8 m. The  $Fe_{PP}$  content in the organic-rich clay layer was relatively high (Figure 3).

The  $Fe_{DH}$ ,  $Fe_{AO}$ , and  $Fe_{PP}$  contents of the borehole C3 sediments were 6.07–27.87 (~average value = 17.58), 3.16–27.71 (~average value = 14.23), and 0.25–2.42 (~average value = 0.67) mg/g, respectively. Among the three boreholes, the overall Fe content in sediment samples from borehole C3 was the lowest. The  $Fe_{AO}$  content exceeded the  $Fe_{DH}$  content at a depth of about −11 m. Similar to the phenomena of boreholes C1 and C2, the  $Fe_{PP}$  content increased in the organic-rich clay layer (Figure 4).

#### 4.2. Variation in Hydrochemical Components in Pore Water with Depth

The variations in anion and cation concentrations in three boreholes' pore water samples with depth are shown in Figures S1–S3 in the Supplementary Materials. According to the hydrochemical analysis, most pore water samples were slightly alkaline and classified as Ca- $HCO_3$  type water except for individual surface samples influenced by human activities (Table 2; Figure 5). The low permeability of clay inhibited the  $O_2$  and DO input, and pore water Eh values decreased with depth (Table 2). The Eh values of shallow pore water in the transitional area (borehole C2) and intense reclamation area (borehole C3) were significantly higher than those in the lake area (borehole C1), which was attributed to changes in the shallow sedimentary environment caused by reclamation.

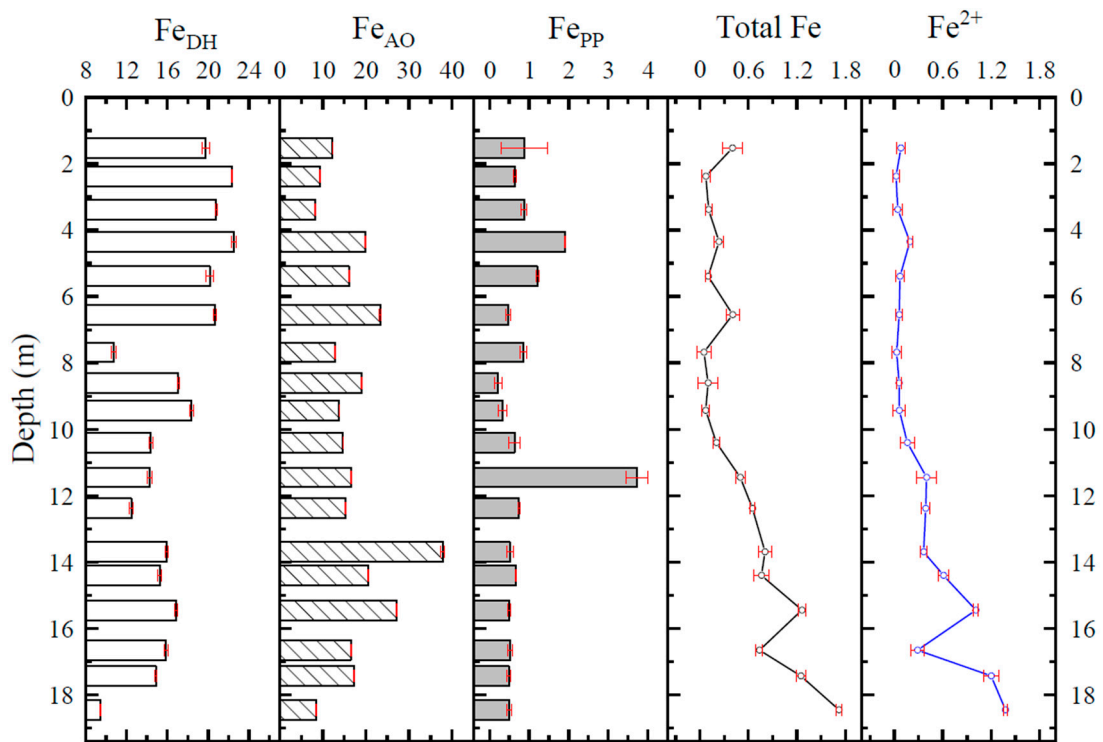


**Figure 2.** Variation in sediment Fe<sub>DH</sub>, Fe<sub>AO</sub>, and Fe<sub>PP</sub> contents (mg/g), and pore water total Fe and Fe<sup>2+</sup> concentrations (mg/L) with depth in borehole C1.

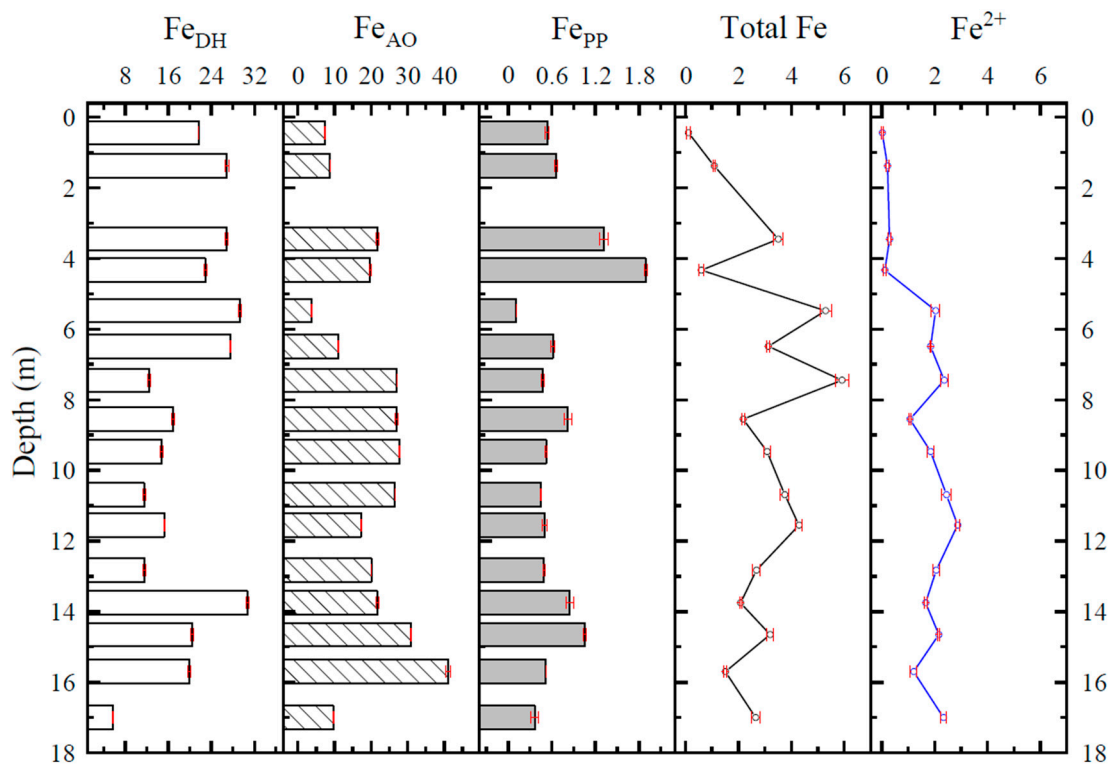


**Figure 3.** Variation in sediment Fe<sub>DH</sub>, Fe<sub>AO</sub>, and Fe<sub>PP</sub> contents (mg/g), and pore water total Fe and Fe<sup>2+</sup> concentrations (mg/L) with depth in borehole C2.

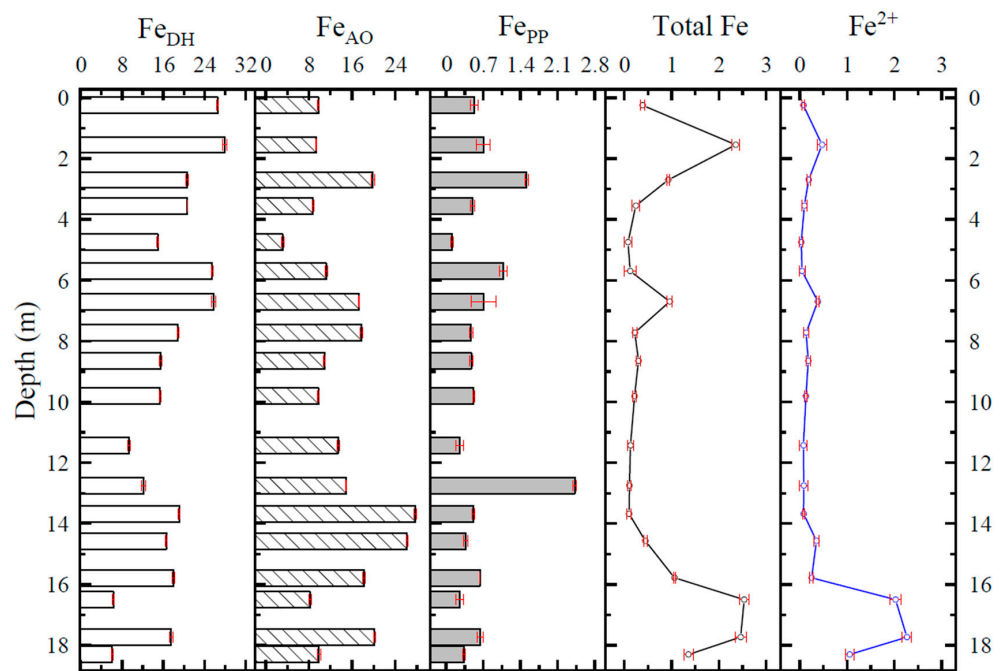


**Figure 4.** Variation in sediment  $Fe_{DH}$ ,  $Fe_{AO}$ , and  $Fe_{PP}$  contents (mg/g) and pore water total Fe and  $Fe^{2+}$  concentrations (mg/L) with depth in borehole C3.

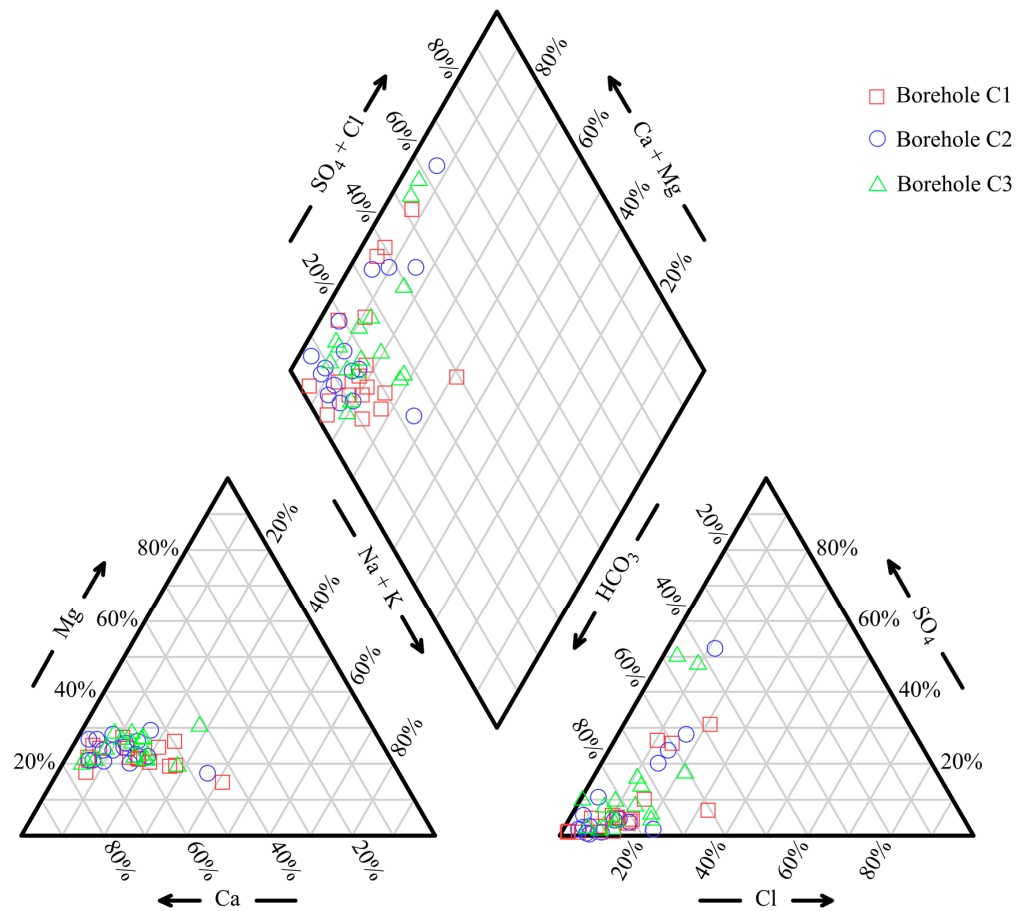


**Figure 5.** Piper diagram of pore water samples in three boreholes.

The total Fe and  $Fe^{2+}$  concentrations in borehole C1 pore water samples were 0.05–1.72 (~average value = 0.52) mg/L and 0.02–1.38 (~average value = 0.36) mg/L, respectively.

Both increased substantially with the depth below about  $-10$  m (Figure 2). The total Fe and  $\text{Fe}^{2+}$  concentrations in borehole C2 pore water samples were  $0.11$ – $5.92$  (~average value =  $2.82$ ) mg/L and  $0.02$ – $2.87$  (~average value =  $2.54$ ) mg/L, respectively. Their overall concentrations were higher among the three boreholes and fluctuated significantly with depth (Figure 3). The total Fe and  $\text{Fe}^{2+}$  concentrations in borehole C3 pore water samples were  $0.08$ – $2.53$  (~average value =  $0.78$ ) mg/L and  $0.03$ – $2.26$  (~average value =  $0.44$ ) mg/L, respectively. Their concentrations were lower in sandy clay, which was consistent with the lower contents of Fe oxides (Figure 4).

The total Fe concentrations in pore water samples were all higher than the World Health Organization's (WHO's) guideline limit ( $0.3$  mg/L), especially at the aquitard–aquifer junction, where the pore water Fe concentration was relatively high throughout the profile. The release of clay pore water inevitably deteriorates the quality of groundwater in the underlying aquifer, posing a health risk for residents.

#### 4.3. Stable Organic Carbon Isotopic Compositions

The stable C isotopic composition ( $\delta^{13}\text{C}$ ) of DOC was analyzed to identify the input differences of surface materials in the deep environment. The  $\delta^{13}\text{C}$  isotope compositions of surface water, irrigation water, sediments, and groundwater in monitoring holes ( $-5$  m,  $-10$  m, and  $-20$  m) are shown in Figure 6.

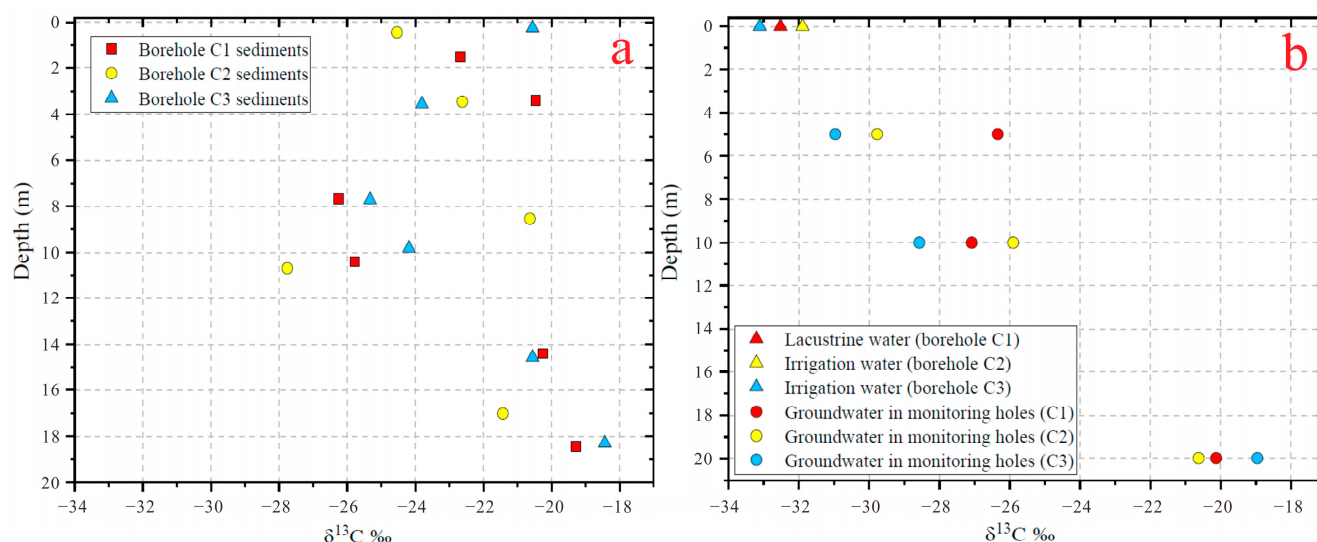


**Figure 6.** The  $\delta^{13}\text{C}$  isotope compositions of (a) Sediments and (b) Surface and groundwater in monitoring holes.

#### 4.4. Result of Excitation Emission Matrices (EEM) Analysis

The EEM contours of three representative pore water samples are shown in Figure 7 since most of our diluted samples exhibited similar spectral structures, and spectral intensity is associated with the DOC content [35]. The fluorescence spectra of DOM in borehole C1 pore water samples were all single-peak humic-like fluorophores, as shown in Figure 7a. A protein-like DOM fluorophore was observed in surface pore water samples from boreholes C2 (above  $-1.38$  m) and C3 (above  $-3.55$  m), as shown in Figure 7b, while the remaining samples exhibited a humic-like fluorophore (Figure 7a).

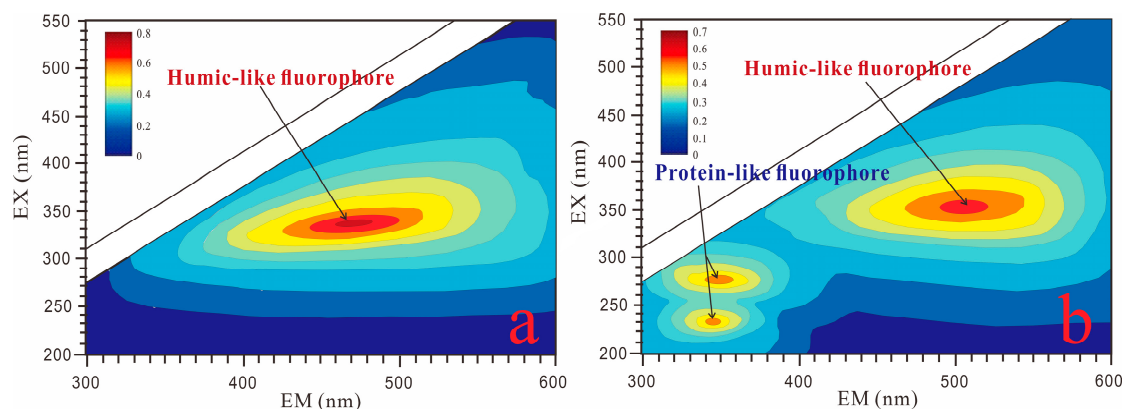


**Figure 7.** Excitation emission matrices (EEM) and contours of DOM measured in pore water samples. (a) Pore water sample from borehole C3 at 3.55 m; (b) Pore water sample from borehole C1 at 3.38 m.

## 5. Discussion

### 5.1. Vertical Distribution and Environmental Factors Influencing Fe in Clayey Aquitard

Clayey aquitard Fe was generated during the transport and deposition of weathered soil parent materials through rivers or lakes. The total Fe and Fe oxide levels in sediments varied irregularly with depth due to the various Fe background values of Fe (Table 2, Figures 2–4). In an oxidation environment, Fe ions in pore water tended to precipitate to form poorly crystalline Fe (III) oxides ( $\text{Fe}_{\text{AO}}$ ), which were later dehydrated and dehydroxylated to generate crystalline Fe (hydrogen) oxides, resulting in higher  $\text{Fe}_{\text{DH}}$  contents in the shallow layers of three boreholes. In a deep reduction environment, abiotic components and dissimilatory metal-reducing bacteria (DMRB) could reduce Fe oxides [36]. Fe (III) oxides become terminal electron receptors for microorganism anaerobic respiration [37]. Even high-crystalline Fe (III) undergoes reductive dissolution, resulting in the generation of  $\text{Fe}^{2+}$  in pore water. Amorphous Fe ( $\text{Fe}_{\text{AO}}$ ) can combine carbonate, clay minerals, OM, and other substances due to its large surface area, which inhibits the growth of the Fe oxide crystal nucleus and its transport into pore water. Therefore, the  $\text{Fe}_{\text{AO}}$  content exceeded the  $\text{Fe}_{\text{DH}}$  content at a certain depth in all three boreholes.

Various environmental factors such as temperature, moisture, pH, Eh, and OM content influence transformation among different Fe minerals in surface soil [38]. The temperature fluctuation in the clayey aquitard is quite minimal in comparison to the surface environment, and their environmental parameters, such as moisture content, also vary significantly. The correlation analyses between Fe components and other chemical indicators of sediments and pore water were conducted using SPSS 25.0 software to identify the influence factors of Fe transformation (Table 3).

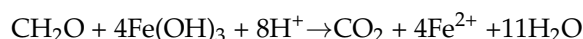
The pore water  $\text{Fe}^{2+}$  concentrations in the three boreholes are all significantly and positively correlated with Eh values. Meanwhile, the  $\text{Fe}^{2+}$ /total Fe ratios (0.15–0.92) increased with depth, indicating that the reductive environment promoted the reduction dissolution of Fe (III) minerals, and  $\text{Fe}^{2+}$  became the predominant Fe form in pore water. Furthermore, due to the significant negative correlation between  $\text{Fe}_{\text{DH}}$  and  $\text{Fe}^{2+}$  concentrations in boreholes C1 and C2, free Fe (III) oxides could be the primary form of Fe that undergoes reduction dissolution. In borehole C3, intense reclamation may obscure the transformation relationship between sediment  $\text{Fe}_{\text{DH}}$  and pore water  $\text{Fe}^{2+}$ . The  $\text{Fe}_{\text{DH}}$  content in borehole C2 was relatively high, resulting in a higher average concentration of total Fe and  $\text{Fe}^{2+}$  in pore water (Figure 3).

**Table 3.** Correlation coefficients between sediment moisture content, Fe oxides, TOC levels, and pore water pH, Eh, DOC, DIC, total Fe, Fe<sup>2+</sup> levels.

Borehole C1	Moisture Content	pH	Eh	TOC	DOC	DIC	Total Fe	Fe <sup>2+</sup>
Fe <sub>DH</sub>	0.589 **	0.115	0.512 *	0.420 *	−0.359	−0.546 *	−0.526 *	−0.537 *
Fe <sub>AO</sub>	0.154	0.206	−0.287	−0.171	0.229	0.148	0.180	0.328
Fe <sub>PP</sub>	0.278	0.103	−0.223	0.314	0.301	0.120	−0.149	−0.092
Toal Fe	−0.248	−0.260	−0.402 *	−0.125	0.495 *	0.648 **	1.000	0.952 **
Fe <sup>2+</sup>	−0.269	−0.263	−0.617 **	−0.066	0.597 **	0.706 **	0.952 **	1.000
Borehole C2	Moisture content	pH	Eh	TOC	DOC	DIC	Total Fe	Fe <sup>2+</sup>
Fe <sub>DH</sub>	0.242	−0.040	0.474 *	0.224	−0.411	−0.528 *	−0.197	−0.501 *
Fe <sub>AO</sub>	−0.266	0.203	−0.324	0.321	0.109	0.242	0.046	0.145
Fe <sub>PP</sub>	0.078	0.159	−0.208	0.647 **	−0.453 *	−0.346	−0.416	−0.563 *
Toal Fe	−0.339	−0.014	−0.336	−0.137	0.485 *	0.482 *	1.000	0.733 **
Fe <sup>2+</sup>	−0.090	0.282	−0.558 **	−0.435 *	0.543 *	0.736 **	0.733 **	1.000
Borehole C3	Moisture content	pH	Eh	TOC	DOC	DIC	Total Fe	Fe <sup>2+</sup>
Fe <sub>DH</sub>	0.513 *	−0.312	0.355	0.560 **	−0.347	−0.288	−0.073	−0.370
Fe <sub>AO</sub>	0.048	0.007	−0.123	0.021	0.206	0.164	−0.048	0.010
Fe <sub>PP</sub>	0.076	0.208	−0.032	0.486 *	0.037	−0.052	−0.118	−0.191
Toal Fe	−0.210	0.045	−0.256	−0.023	0.465 *	0.518 *	1.000	0.847 **
Fe <sup>2+</sup>	−0.409	0.248	−0.478 *	−0.188	0.545 **	0.521 *	0.847 **	1.000

Note(s): \* Significance < 0.05; \*\* Significance < 0.01.

According to the results of correlation analysis, the pore water's pH had no significant impact on the transformation of sediment Fe. The moisture content showed a similar variation trend to the Fe<sub>DH</sub> content with depths in boreholes C1 and C3, but it had a limited effect on Fe enrichment in pore water. Apart from Eh, lithology and the OM content also affected the Fe concentrations of sediments and pore water. The OM content was relatively high in the organic-rich clay layer, resulting in a higher content of complex Fe (Fe<sub>PP</sub>). In boreholes C2 and C3, the Fe<sub>PP</sub> contents were significantly positively correlated with the sediment TOC contents. OM is one of the main electron donors for the dissimilatory reduction in Fe (III). Taking CH<sub>2</sub>O as an example, the reaction equation is as follows:



Small molecule organic carbon and CO<sub>2</sub> generated by OM mineralization become the sources of DOC and DIC in pore water [12]. The significant positive correlations between DOC, DIC, and Fe<sup>2+</sup> concentrations confirm the importance of OM in Fe (III) reduction dissolution (Table 3). The average content of sediment TOC (8.18 mg/g) in borehole C2 was higher than those in boreholes C1 (6.70 mg/g) and C3 (7.02 mg/g), which could explain why borehole C2 had the highest average concentration of pore water Fe ions. The muddy sand (−9.7–−6.0 m) and sandy clay (depth −14.9–−9.7 m) layers exposed by borehole C3 had a high sand content, strong permeability, and insufficient water–rock interactions. The main component of sandy minerals was SiO<sub>2</sub>, which did not absorb Fe ions and DOM-like negatively charged clay minerals [4], so the overall Fe and Fe<sup>2+</sup> concentrations of this layer were low (Figure 4).

### 5.2. Effect of Reclamation on Fe Occurrence in Clayey Aquitard

The moisture content of surface sediments (>−3 m) in boreholes C2 and C3 were lower than those in borehole C1, but the average values of DO (C1: 3.85, C2: 5.89, C3: 6.65 ppm) and Eh for surface pore water were higher (Table 2). Reclamation drained the

surface water around the locations of boreholes C2 and C3 and destroyed the surface sediment's structure, intensifying water evaporation and oxygen input.

The average  $\text{Fe}_{\text{AO}}/\text{Fe}_{\text{DH}}$  content ratios of surface sediments ( $> -3$  m) in boreholes C2 and C3 were lower than in borehole C1 (C1: 0.52, C2: 0.33, C3: 0.35), indicating that the low moisture content and strong oxidation environment caused by reclamation promoted the transformation of amorphous Fe to high-crystalline Fe. Meanwhile, the  $\text{Fe}_{\text{DH}}$  content of surface sediments was the highest in borehole C3, which could explain the depth in borehole C3 where the  $\text{Fe}_{\text{AO}}$  content that exceeded  $\text{Fe}_{\text{DH}}$  was deeper. Surface pore water pH values ( $> -3$  m) in boreholes C2 and C3 were lower than in borehole C1 (Table 2), but the orders of EC average values (C1: 594.4, C2: 712.6, C3: 819.8  $\mu\text{S}/\text{cm}$ ) and  $\text{HCO}_3^-$  average concentrations (C1: 143.82, C2: 228.04, C3: 290.53 mg/L) were opposite. These findings suggest that the disruption of sediment texture structure during reclamation accelerated the  $\text{CO}_2$  input and evaporation concentration, resulting in higher  $\text{Fe}^{3+}$  concentrations in boreholes C2 and C3's pore water samples (Figures 3 and 4).

Based on water level monitoring data, the groundwater level fluctuated by 17.30–21.88 m. The groundwater levels in borehole C1 aquitard were mostly higher than those in the aquifer throughout the year, suggesting a downward hydraulic gradient from the aquitard to the aquifer. This is consistent with the reported groundwater simulation results in the JHP [39]. The average downward hydraulic gradients of clayey aquitard in boreholes C1, C2, and C3 during the monitoring period were 0.045, 0.097, and 0.104, respectively. The vertical flow rate through the shallow aquitard to the aquifer was estimated to be from 0.1 to 1.0 m/year via multiple means [39–41]. Lei et al. discovered a hydraulic connection between the shallow aquitard and aquifer using  $^2\text{H}-^{18}\text{O}$  isotopes in Chen Lake wetland and the reclamation extended groundwater flow paths [42]. In summary, surface reclamation may have an impact on subsurface geochemical processes via environmental disturbances and chemical substance inputs.

According to the  $\delta^{13}\text{C}$  isotope test results (Figure 6), the organic carbon in pore water at different depths had distinct sources. For borehole C1, the  $\delta^{13}\text{C}$  of groundwater in the monitoring holes at  $-5$  m and  $-10$  m ranged between the  $\delta^{13}\text{C}$  of lacustrine water and in situ sediments, indicating that the DOC at these two depths was derived from mixed sources. The  $\delta^{13}\text{C}$  of groundwater at  $-20$  m was close to the  $\delta^{13}\text{C}$  of sediments at  $-18.45$  m. Considering the vertical flow in clayey aquitard, the DOC in the groundwater at a  $-20$  m depth probably originated from the in situ dissolution of sediment organic carbon. Boreholes C2 and C3 had similar sources of groundwater DOC at depths of  $-5$  m,  $-10$  m, and  $-20$  m to borehole C1. However, the  $\delta^{13}\text{C}$  contents at a  $-5$  m depth in borehole C2 and  $-5$  m and  $-10$  m depths in borehole C3 were lower than those at corresponding depths in borehole C1, indicating a greater contribution of DOC from surface water in these two boreholes (C2 and C3).

Reclamation had little effect on the background value of Fe in the clayey aquitard, but some DOM could enter deep into the strata with the infiltration of groundwater, resulting in electron donors for Fe (III) reduction. Based on the test results of EEM, the pore water DOM in borehole C1 was all humic-like OM under long-term humification (Figure 7). The appearance of protein-like DOM fluorophores in surface pore water samples from boreholes C2 and C3 suggest that cultivated crops present incompletely humified OM to the clay layer, which could be preferentially utilized by microorganisms to provide electrons for Fe reduction [12]. As a result of the OM input from the cultivated crops, borehole C3 had higher average levels of TOC (Table 2) and DOC (C1: 8.84, C2: 9.55, C3: 14.83 mg/L) above  $-3$  m than boreholes C1 and C2, which might promote the enrichment of pore water Fe ions.

### 5.3. Potential Migration and Transformation Mechanisms of Fe during the Evolution of Clayey Aquitard

Taking the borehole C1 pore water samples, which were less affected by human activities, as an example, PHREEQC Version 3 software was used to simulate and calculate the

saturation index ( $SI = \log IAP/K_{sp}$ ) of different Fe minerals. Based on the precipitation or dissolution of different Fe minerals, the potential transformation process of Fe in clayey aquitard was further identified. The pH, cations ( $K^+$ ,  $Na^+$ ,  $Ca^{2+}$ ,  $Mg^{2+}$ ,  $Al^{3+}$ ,  $Fe^{3+}$ ,  $Fe^{2+}$ ,  $Mn^{2+}$ ), and anions ( $Cl^-$ ,  $SO_4^{2-}$ ,  $HCO_3^-$ ,  $NO_3^-$ ,  $PO_4^{3-}$ ,  $S^{2-}$ ) at different depths were applied to calculate the saturation indices of six Fe minerals (ferrihydrite ( $Fe_5HO_8 \cdot 4H_2O$ ), lepidocrocite ( $FeOOH$ ), magnetite ( $Fe_3O_4$ ), goethite ( $Fe(OH)_3$ ), siderite ( $FeCO_3$ ) and mackinawite ( $FeS$ )) (Figure 8). Among them, ferrihydrite and lepidocrocite belong to amorphous Fe (III), which can be further matured into high-crystalline Fe (III), such as goethite and magnetite. Siderite and mackinawite belong to Fe (II) minerals.

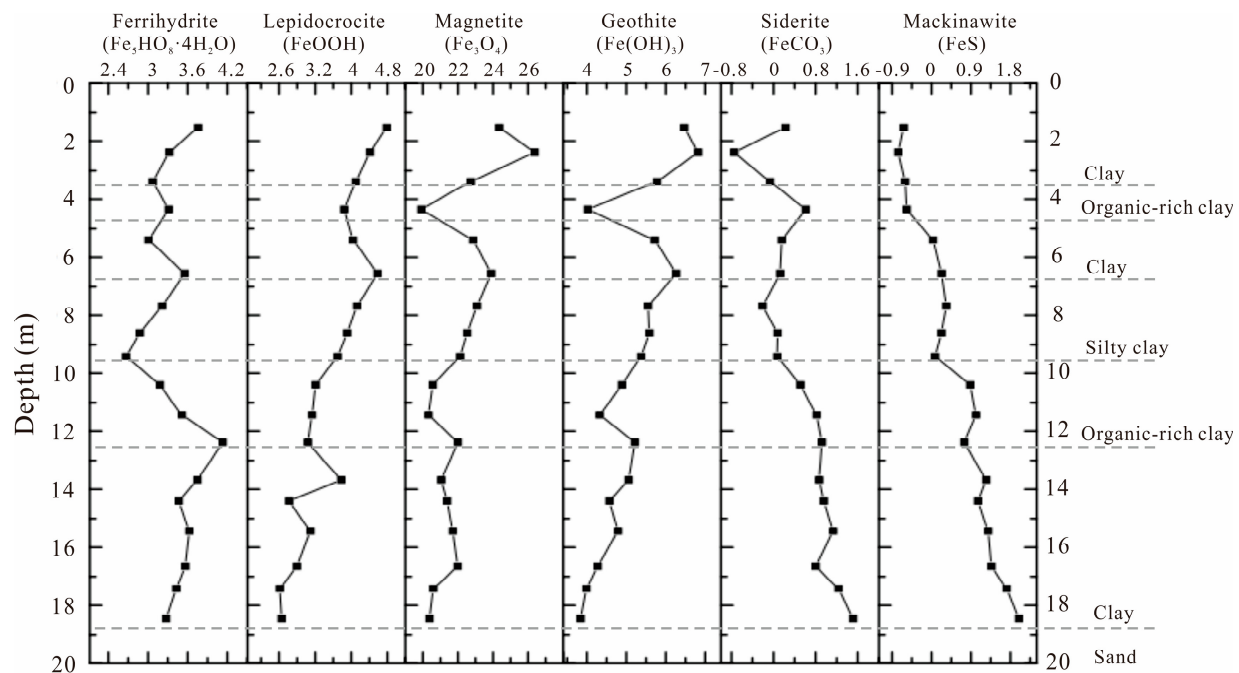


**Figure 8.** Variation in saturation indices of different Fe minerals with depth in borehole C1.

In the shallow oxidative environment ( $-3.5$ – $0$  m), the saturation indices of ferrihydrite and lepidocrocite decreased with depth, while the saturation indices of magnetite and goethite initially increased with depth, indicating the occurrence of Fe crystallization. Poor crystalline Fe (III) transforms to a highly crystalline state via (1) dissolution and recrystallization: the hydroxyl-Fe ions such as  $Fe(OH)^+$  and  $Fe(OH)^{2+}$  produced by ferrihydrite dissolution, polymerize, and precipitate transform to crystalline Fe (hydrogen) oxides. (2) Internal solid-phase transformation also occurs: the rearrangement of atomic structures in ferrihydrite's crystal structure is accompanied by dehydration or dehydroxylation [43]. The saturation indices of magnetite and goethite both decreased after entering the reductive environment in the first organic-rich clay layer ( $-4.7$ – $-3.5$  m), which could be related to the dissimilatory reduction in Fe (III) induced by a high OM content. However, the saturation indices of ferrihydrite and lepidocrocite did not change significantly, possibly because they absorbed other chemicals to form a closed storage structure and inhibit the dissimilatory reduction. In the second clay layer ( $-6.8$ – $-4.7$  m), due to the high background contents of  $Fe_{DH}$  and  $Fe_{AO}$  (Figure 2), the saturation indices of Fe (III) minerals all increased with depth. Below  $-6.8$  m, the saturation indices of lepidocrocite, magnetite, and goethite all decreased with depth, indicating that both poorly crystalline and crystalline Fe oxides were reduced, resulting in an enrichment of  $Fe^{2+}$  in pore water with depth. In the second organic-rich clay layer ( $-12.5$ – $-9.5$  m), the saturation index of ferrihydrite gradually increased with depth, corresponding to the high content of  $Fe_{PP}$  and indicating that it might combine with OM.

The saturation indices of siderite and mackinawite in the shallow clay layer ( $-3.5$ – $0$  m) were generally negative, indicating that Fe (II) minerals were dissolved. Below  $-3.5$  m,

their saturation indices increased in fluctuation with depth and exceeded 0, indicating that the  $\text{Fe}^{2+}$  generated by Fe (III) reduction can interact with  $\text{CO}_3^{2-}$  and  $\text{S}^{2-}$  to form a precipitate, and the potential for generating Fe (II) precipitation increased with depth.

#### 5.4. Ecological Effects of Fe (III) Reduction in Clayey Aquitard

The variations in trace element concentrations in three borehole pore water samples with depth are shown in Figures S4–S6 in the Supplementary Materials. To identify the effect of Fe reduction dissolution on the release of other chemical components in clayey sediments, the relationship between Fe and As, Ba, Cd, Co, Cr, Cu, Mn, Ni, Pb, Rb, Sr, V, and Zn in the whole pore water samples was described using correlation analysis and principal component analysis (PCA) (Table 4, Figure 9). The Kaiser–Meyer–Olkin (KMO) and Bartlett’s tests were performed to assess the suitability of the data and the independence of variables. KMO is a measure of sampling adequacy that indicates whether the variables can be grouped into a smaller set of potential factors. The KMO of the analysis result exceeded 0.5, indicating that the data were suitable for PCA; Bartlett’s test yielded a significance level of  $< 0.05$  (near 0), indicating that there could be a statistically significant interrelationship between these variables. PCA showed that As, Cr, Sr, Zn, and Mn were strongly associated with  $\text{Fe}^{2+}$  and total Fe for PC1 (Figure 9), and the concentrations of As, Cr, Sr, Zn, and Mn were significantly and positively correlated with the  $\text{Fe}^{2+}$  concentration (Table 4). Based on the results from the correlation analysis and PCA, the release of sediments As, Cr, Sr, Zn, and Mn to pore water could be associated with Fe reduction processes.

**Table 4.** Correlation coefficients between total Fe,  $\text{Fe}^{2+}$ , and trace element concentrations in pore water.

	As	Ba	Cd	Co	Cr	Cu	Mn
Total Fe	0.519 **	0.081	0.013	0.140	0.538 **	−0.258	0.239
$\text{Fe}^{2+}$	0.752 **	0.269	0.045	0.194	0.647 **	−0.305	0.450 **
	Ni	Pb	Rb	Sr	V	Zn	
Total Fe	−0.164	0.095	0.095	0.555 *	−0.056	0.640 **	
$\text{Fe}^{2+}$	−0.366	0.236	−0.081	0.682 **	−0.033	0.659 **	

Note(s): \* Significance  $< 0.05$ ; \*\* Significance  $< 0.01$ .

Hydroxyl groups can form exchanges with other ligands as metal ion ligands and act as flocculants in sediments to promote the formation of macroaggregates. Amorphous Fe is rich in active hydroxyl groups and is an important adsorbent for elements such as As due to its large specific surface area and high surface activity [44]. Sediment heavy metals could be released with the reduction dissolution of Fe oxides [45] as one of the main sources of heavy metals in pore water. However, statistical analysis alone cannot adequately demonstrate the release mechanism of heavy metals, and future research should focus on the morphological changes of heavy metals in sediments (such as the Fe-bound form).

Hence, we must pay more attention to drinking or using groundwater with high concentrations of Fe and exploiting groundwater reasonably to avoid clayey sediment compaction induced by the level of the waterfall.

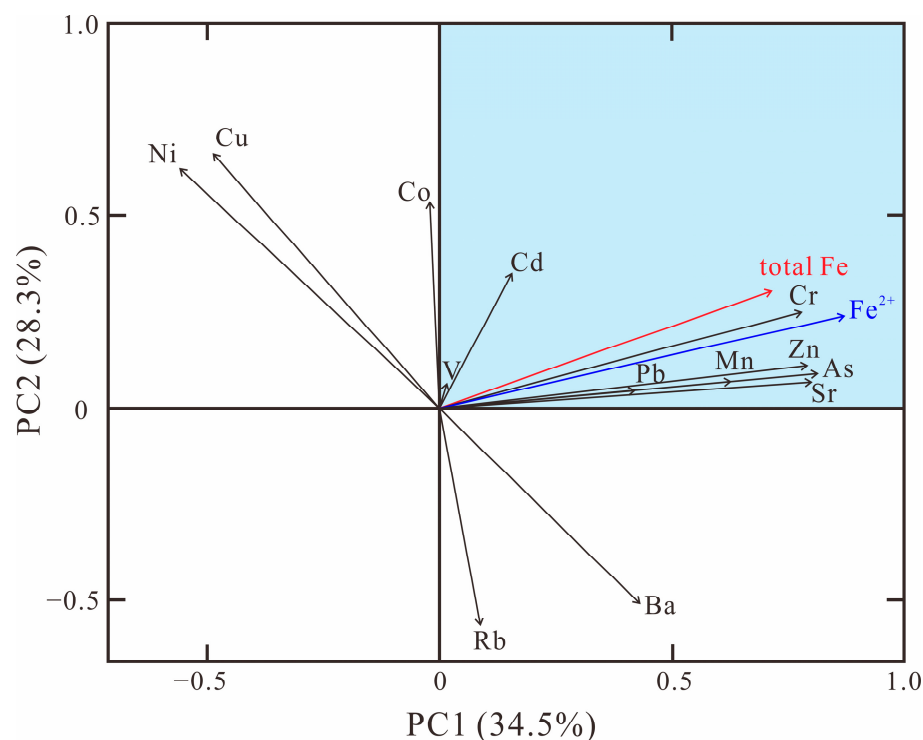


**Figure 9.** PCA biplots represent the factor loadings of the first two components (PC-1 and PC-2) in all pore water samples.

## 6. Conclusions

The lithology of alluvial–lacustrine sediments mainly control the Fe content in the clayey sediment, and the transformation form is primarily free Fe (III) oxides, which is one of the main sources of pore water Fe. The higher OM content is advantageous for the dissimilatory reduction in Fe (III) oxides in the organic-rich clay layers. The pore water Fe concentration increases with depth, which is significantly higher than the WHO guideline’s limit at the aquitard–aquifer junction, posing a threat to the safety of drinking water for residents.

Reclamation mainly changes the surface sedimentary environment. The low moisture content and pore water pH, as well as the intense oxidative environment, promote the crystallization of Fe minerals. The OM input from crops into the deep environment becomes an essential electron donor for the dissimilatory reduction in Fe (III), enhancing the transformation potential of sediment Fe into pore water. The high content of Fe<sup>2+</sup> in deep pore water promotes the precipitation of Fe (II) minerals. Different Fe (III) minerals all tend to dissolve with increasing depth. The concentrations of As, Cr, Sr, Zn, and Mn in pore water varied similarly to the Fe concentration, and their release could be attributed to the reduction dissolution of sediment Fe oxides.

**Supplementary Materials:** The following supporting information can be downloaded at: <https://www.mdpi.com/article/10.3390/w15223934/s1>, Figure S1: Variation of hydrochemical components concentrations in borehole C1 pore water samples with depth; Figure S2: Variation of hydrochemical components concentrations in borehole C2 pore water samples with depth; Figure S3: Variation of hydrochemical components concentrations in borehole C3 pore water samples with depth; Figure S4: Variation of trace elements concentrations in borehole C1 pore water samples with depth; Figure S5: Variation of trace elements concentrations in borehole C2 pore water samples with depth; Figure S6: Variation of trace elements concentrations in borehole C3 pore water samples with depth.

**Author Contributions:** Methodology, R.L.; Formal analysis, R.L.; Investigation, J.C. and Y.J.; Data curation, Y.J.; Writing—original draft preparation, J.C.; Writing—review and editing, T.M. All authors have read and agreed to the published version of the manuscript.

**Funding:** This research was funded by the National Natural Science Foundation of China (grant number 41630318, 42007173); Research & Development Foundation of China Institute of Geo-Environment Monitoring (grant number 20230101).

**Data Availability Statement:** The data presented in this study are available on request from the corresponding author. The data are not publicly available due to data acquisition program was performed from other public organization.

**Acknowledgments:** The authors would like to express sincere appreciation to the reviewers and editor for their comments and editorial service.

**Conflicts of Interest:** There are no conflict of interest to declare.

## References

1. Hendry, M.J.; Woodbury, A.D. Clay Aquitards as Archives of Holocenepaleo Climate:  $\delta^{18}\text{O}$  and Thermal Profiling. *Groundwater* **2007**, *45*, 683–691. [[CrossRef](#)] [[PubMed](#)]
2. Jiao, J.; Wang, Y.; Cherry, J.A.; Wang, X.; Zhi, B.; Du, H.; Wen, D. Abnormally High Ammonium of Natural Origin in a Coastal Aquifer-Aquitard System in the Pearl River Delta, China. *Environ. Sci. Technol.* **2010**, *44*, 7470–7475. [[CrossRef](#)] [[PubMed](#)]
3. Mihajlov, I.; Mozumder, M.R.H.; Bostick, B.C.; Stute, M.; Mailloux, B.J.; Knappett, P.S.; Choudhury, I.; Ahmed, K.M.; Schlosser, P.; Geen, A.V. Arsenic Contamination of Bangladesh Aquifers Exacerbated by Clay Layers. *Nat. Commun.* **2020**, *11*, 2244. [[CrossRef](#)] [[PubMed](#)]
4. Qiu, W.; Ma, T.; Liu, R.; Du, Y. Variations in the Mineral Structures Dominating Solute Mobilization during Clay Compaction. *J. Hydrol.* **2022**, *610*, 127843. [[CrossRef](#)]
5. Potter, P.E.; Maynard, J.B.; Depetris, P.J. Mud and Mudstones: Introduction and Overview. *Econ. Geol.* **2005**, *100*, 1469–1471.
6. Wang, Y.; Jiao, J.J.; Cherry, J.A.; Lee, C. Contribution of the Aquitard to the Regional Ground Water Hydrogeochemistry of the Underlying Confined Aquifer in the Pearl River Delta, China. *Sci. Total Environ.* **2013**, *461–462*, 663–671. [[CrossRef](#)]
7. Konikow, L.F.; Kendy, E. Groundwater Depletion: A Global Problem. *Hydrogeol. J.* **2005**, *13*, 317–320. [[CrossRef](#)]
8. Beylich, A.; Oberholzer, H.R.; Schrader, S.; Hoper, H.; Wilke, B. Evaluation of Soil Compaction Effects on Soil Biota and Soil Biological Processes in Soils. *Soil Till. Res.* **2010**, *109*, 133–143. [[CrossRef](#)]
9. Smith, R.; Knight, R.; Fendorf, S. Overpumping Leads to California Groundwater Arsenic Threat. *Nat. Commun.* **2018**, *9*, 2089. [[CrossRef](#)] [[PubMed](#)]
10. Li, J.; Wang, Y.; Zhu, C.; Xue, X.; Qian, K.; Xie, X.; Wang, Y. Hydrogeochemical Process Controlling the Mobilization and Enrichment of Fluoride in Groundwater of the North China Plain. *Sci. Total Environ.* **2020**, *730*, 138877. [[CrossRef](#)]
11. Hendry, M.J.; Wassenaar, L.I. Transport and geochemical controls on the distribution of solutes and stable isotopes in a thick clay-rich till aquitard, Canada. *Isotopes Environ. Health Stud.* **2004**, *40*, 3–19. [[CrossRef](#)] [[PubMed](#)]
12. Liu, R.; Ma, T.; Qiu, W.; Du, Y.; Liu, Y. Effects of Fe Oxides on Organic Carbon Variation in the Evolution of Clayey Aquitard and Environmental Significance. *Sci. Total Environ.* **2020**, *701*, 134776. [[CrossRef](#)] [[PubMed](#)]
13. Guo, W.; Cecchetti, A.R.; Wen, Y.; Zhou, Q.; Sedlak, D.L. Sulfur Cycle in a Wetland Microcosm: Extended S-34-Stable Isotope Analysis and Mass Balance. *Environ. Sci. Technol.* **2020**, *54*, 5498–5508. [[CrossRef](#)] [[PubMed](#)]
14. Tao, Y.; Deng, Y.; Du, Y.; Xu, Y.; Leng, Z.; Ma, T.; Wang, Y. Sources and Enrichment of Phosphorus in Groundwater of the Central Yangtze River Basin. *Sci. Total Environ.* **2020**, *737*, 139837. [[CrossRef](#)] [[PubMed](#)]
15. Abdelrady, A.; Sharma, S.; Sefelnasr, A.; Kennedy, M. Characterisation of the Impact of Dissolved Organic Matter on Iron, Manganese, and Arsenic Mobilisation during Bank Filtration. *J. Environ. Manage.* **2020**, *258*, 110003. [[CrossRef](#)]
16. Xu, D.; Hu, S.; Xiong, Y.; Yang, Y.; Ran, Y. Importance of the Structure and Micropores of Sedimentary Organic Matter in the Sorption of Phenanthrene and Nonylphenol. *Environ. Pollut.* **2020**, *260*, 114034. [[CrossRef](#)]
17. Xing, G.; Garg, S.; Miller, C.J.; Pham, A.N.; Waite, T.D. Effect of Chloride and Suwannee River Fulvic Acid on Cu Speciation: Implications to Cu Redox Transformations in Simulated Natural Waters. *Environ. Sci. Technol.* **2020**, *54*, 2334–2343. [[CrossRef](#)]
18. Nickson, R.T.; McArthur, J.M.; Ravenscroft, P.; Burgess, W.G.; Ahmed, K.M. Mechanism of Arsenic Release to Groundwater, Bangladesh and West Bengal. *Appl. Geochem.* **2000**, *15*, 403–413. [[CrossRef](#)]
19. Mueller, B.; Hug, S.J. Climatic Variations and De-Coupling between Arsenic and Iron in Arsenic Contaminated Ground Water in the Lowlands of Nepal. *Chemosphere* **2018**, *210*, 347–358. [[CrossRef](#)]
20. Erban, L.E.; Gorelick, S.M.; Zebker, H.A.; Fendorf, S. Release of Arsenic to Deep Groundwater in the Mekong Delta, Vietnam, Linked to Pumping-Induced Land Subsidence. *Proc. Natl. Acad. Sci. USA* **2013**, *110*, 13751–13756. [[CrossRef](#)]
21. Liu, R.; Ma, T.; Qiu, W.; Peng, Z.; Shi, C. The Environmental Functions and Ecological Effects of Organic Carbon in Silt. *J. Earth Sci.* **2020**, *31*, 834–844. [[CrossRef](#)]
22. Sharma, G.K.; Jena, R.K.; Ray, P.; Yadav, K.K.; Moharana, P.C.; Cabral-Pinto, M.M.S.; Bordoloi, G. Evaluating The Geochemistry of Groundwater Contamination with Iron and Manganese and Probabilistic Human Health Risk Assessment in Endemic Areas of The World's Largest River Island, India. *Environ. Toxicol. Phar.* **2021**, *87*, 103690. [[CrossRef](#)]
23. Du, Y.; Ma, T.; Deng, Y.; Shen, S.; Lu, Z. Sources and Fate of High Levels of Ammonium in Surface Water and Shallow Groundwater of the Jiangnan Plain, Central China. *Environ. Sci.-Proc. Imp.* **2017**, *19*, 161–172. [[CrossRef](#)]

24. Du, Y.; Deng, Y.; Ma, T.; Lu, Z.; Shen, S.; Gan, Y.; Wang, Y. Hydrogeochemical Evidences for Targeting Sources of Safe Groundwater Supply in Arsenic-Affected Multilevel Aquifer Systems. *Sci. Total Environ.* **2018**, *645*, 1159–1171. [[CrossRef](#)]
25. Xiao, C.; Ma, T.; Du, Y. Arsenic Releasing Mechanisms during Clayey Sediments Compaction: An Experiment Study. *J. Hydrol.* **2020**, *597*, 125743. [[CrossRef](#)]
26. Zhou, J.; Du, Y.; Deng, Y.; Tao, Y.; Leng, Z.; Ma, T.; Wang, Y. Source identification of groundwater phosphorus under different geological settings in the central Yangtze River basin. *J. Hydrol.* **2022**, *612*, 128169. [[CrossRef](#)]
27. Liu, R.; Chen, J.; Ma, T. Releasing mechanism of ammonium during clayey sediments compaction and its impact on groundwater environment. *Sci. Total Environ.* **2023**, *898*, 165579. [[CrossRef](#)] [[PubMed](#)]
28. Gan, Y.; Wang, Y.; Duan, Y.; Deng, Y.; Guo, X.; Ding, X. Hydrogeochemistry and Arsenic Contamination of Groundwater in the Jiangnan Plain, Central China. *J. Geochem. Explor.* **2014**, *138*, 81–93. [[CrossRef](#)]
29. Zhang, J.; Liang, X.; Ge, Q.; Li, H.; Zhu, B. Calculation method about hydraulic conductivity of Quaternary aquitard in Jiangnan Plain. *Earth Sci.-China* **2017**, *42*, 761–770. (In Chinese)
30. Xiao, C.; Ma, T.; Du, Y.; Yu, H.; Shen, S. Arsenic Releasing Characteristics During the Compaction of Muddy Sediments. *Environ. Sci. Process. Impacts* **2016**, *18*, 1297–1304. [[CrossRef](#)]
31. Coward, E.K.; Thompson, A.T.; Plante, A.F. Iron-Mediated Mineralogical Control of Organic Matter Accumulation in Tropical Soils. *Geoderma* **2017**, *306*, 206–216. [[CrossRef](#)]
32. Wagai, R.; Mayer, L.; Kitayama, K.; Shirato, Y. Association of Organic Matter with Iron and Aluminum across A Range of Soils Determined Via Selective Dissolution Techniques Coupled with Dissolved Nitrogen Analysis. *Biogeochemistry* **2013**, *112*, 95–109. [[CrossRef](#)]
33. Parfitt, R.L.; Childs, C.W. Estimation of Forms of Fe and Al: A Review and Analysis of Contrasting Soils by Dissolution and Mossbauer Methods. *Aust. J. Soil Res.* **1988**, *26*, 121–144. [[CrossRef](#)]
34. Loveland, P.J.; Digby, P. The Extraction of Fe and Al By 0.1 M Pyrophosphate Solutions: A Comparison of Some Techniques. *Eur. J. Soil Sci.* **1984**, *35*, 243–250. [[CrossRef](#)]
35. Bekhterev, V.N.; Kabina, E.A. Technology of Vapor-Phase Extraction of Water-Soluble Organic Substances. *Russ. J. Appl. Chem.* **2007**, *80*, 716–721. [[CrossRef](#)]
36. Adhikari, D.; Zhao, Q.; Das, K.; Mejia, J.; Huang, R.; Wang, X.; Poulson, S.R.; Tang, Y.; Roden, E.E.; Yang, Y. Dynamics of Ferrihydrite-Bound Organic Carbon during Microbial Fe Reduction. *Geochim. Cosmochim. Acta* **2017**, *212*, 221–233. [[CrossRef](#)]
37. Lovley, D.R.; Holmes, D.E.; Nevin, K.P. Dissimilatory Fe(III) and Mn(IV) Reduction. *Adv. Microb. Physiol.* **2004**, *49*, 219.
38. Chen, C.; Kukkadapu, R.; Sparks, D.L. Influence of Coprecipitated Organic Matter on Fe<sup>2+</sup>(aq)-Catalyzed Transformation of Ferrihydrite: Implications for Carbon Dynamics. *Environ. Sci. Technol.* **2015**, *49*, 10927–10936. [[CrossRef](#)]
39. Du, Y.; Ma, T.; Deng, Y.; Shen, S.; Lu, Z. Characterizing groundwater/surfacewater interactions in the interior of Jiangnan Plain, central China. *Hydrogeol. J.* **2018**, *26*, 1047–1059. [[CrossRef](#)]
40. Guo, X. Arsenic Mobilization and Transport in Shallow Aquifer Systems of Jiangnan Plain, Central China. Ph.D. Thesis, China University of Geosciences, Wuhan, China, 2014.
41. Schaefer, M.V.; Ying, S.C.; Benner, S.G.; Duan, Y.; Wang, Y.; Fendorf, S. Aquifer arsenic cycling induced by seasonal hydrologic changes within the Yangtze River basin. *Environ. Sci. Technol.* **2016**, *50*, 3521–3529. [[CrossRef](#)]
42. Lei, K.; Ma, T.; Chen, L.; Li, Z.; Chen, Y. Effect of Reclamation on the Groundwater-Lake Water Interaction in Chen Lake. *J. Earth Sci.* **2022**. [[CrossRef](#)]
43. Schwertmann, U.; Friedl, J.; Stanjek, H. From Fe (III) Ions to Ferrihydrite and then to Hematite. *J. Colloid Interf. Sci.* **1999**, *209*, 215–223. [[CrossRef](#)]
44. Hou, T.; Xu, R.; Zhao, A. Interaction between Electric Double Layers of Kaolinite and Fe/Al Oxides in Suspensions. *Colloid Surf. A* **2007**, *297*, 91–94. [[CrossRef](#)]
45. Wang, Y.; Jiao, J.J.; Zhang, K.; Zhou, Y. Enrichment and Mechanisms of Heavy Metal Mobility in a Coastal Quaternary Groundwater System of the Pearl River Delta, China. *Sci. Total Environ.* **2016**, *545–546*, 493–502. [[CrossRef](#)]

**Disclaimer/Publisher's Note:** The statements, opinions and data contained in all publications are solely those of the individual author(s) and contributor(s) and not of MDPI and/or the editor(s). MDPI and/or the editor(s) disclaim responsibility for any injury to people or property resulting from any ideas, methods, instructions or products referred to in the content.